ORIGINAL RESEARCH ARTICLE

Destabilization Treatment and Its Influence on Microstructure and Matrix Hardness of High-Cr Cast Iron

CHARLINE LE NUÉ, SANTIAGO CORUJEIRA GALLO, ALIREZA VAHID, JIANGTING WANG, MEHDI TAHERISHARGH, HOOYAR ATTAR, DANIEL FABIJANIC, and MATTHEW BARNETT

High-chromium cast irons are an essential class of wear-resistant materials commonly used for wear-resistant applications in the mining and steel industries. There is ongoing debate on the secondary carbide types and their formation sequences during heat treatment. This work examines the microstructural evolution during destabilization treatment of a hypoeutectic high-chromium cast iron containing 2.2 wt pct C and 16.5 wt pct Cr. Starting from an inhomogeneous as-cast microstructure consisting of ~ 28 pct M_7C_3 eutectic carbide and a mixed matrix of martensite and retained austenite, destabilization treatments resulted in the establishment of near homogeneous structure with a near equilibrium level of carbon concentration in the matrix, which fully transformed to martensite upon cooling. Homogeneously distributed $M_{23}C_6$ secondary carbides with a square-shaped morphology and 100 to 500 nm in size precipitated during heating up to the destabilization temperature. For higher destabilization temperatures (1000 °C), M_7C_3 secondary carbides formed together with $M_{23}C_6$ and were identifiable by a distinctly different morphology (elongated). It was found that the carbon content of the matrix, a function of the destabilization temperature and subsequent eutectic carbide dissolution, controls the martensite start temperature and has a dominating influence on bulk-hardness.

I. INTRODUCTION

HIGH-CHROMIUM cast irons (HCCI) are commonly used for materials handling in the mining and minerals processing industries due to their excellent abrasion wear resistance. The microstructure in the as-cast state is typically dominated by eutectic carbides M_7C_3 in an austenitic matrix. Castings are generally heat-treated to enhance wear performance. One of the main aims is to destabilize the austenite to a sufficient extent for martensite to form throughout the structure upon cooling to room temperature. For this reason, heat treatments are often termed destabilization treatments.

They are usually conducted at 800 °C to 1100 °C for 1 to 6 hours, leading to extensive precipitation of secondary carbides and austenite transformation into martensite upon cooling.

Numerous studies have focused on the influence of destabilization treatment on the microstructure.[1–6] Nevertheless, discrepancies still exist concerning the stability of eutectic carbides and secondary carbide type and precipitation sequence, particularly for alloys having an intermediate Cr/C ratio (5.8 to 11), with Cr contents typically in the 16 to 28 wt pct Cr range. Some studies report that M_7C_3 eutectic carbides do not appear to be significantly modified during the destabilization heat treatment,[2,3,7–11] whereas other reports their partial dissolution.[1,12–14] For higher Cr content, outside of our interested range (around 30 wt pct Cr), authors observe the partial transformation of eutectic carbides M_7C_3 into $M_{23}C_6$.[15–17] The secondary carbide precipitation sequence is also contentious. Some authors report the formation of M_7C_3 secondary carbides only,[2,10,11,18,19] others observed exclusively $M_{23}C_6$ secondary carbides,[14,20–23] whereas others reported a mix of both M_7C_3 and $M_{23}C_6$ secondary carbides.[1,5,11,24,25]

CHARLINE LE NUÉ, SANTIAGO CORUJEIRA GALLO, ALIREZA VAHID, JIANGTING WANG, DANIEL FABIJANIC, and MATTHEW BARNETT are with the Institute for Frontier Materials, Deakin University, Geelong, VIC 3216, Australia. Contact e-mail: c.lenue@deakin.edu.au MEHDI TAHERISHARGH and HOOYAR ATTAR are with the Bradken, Mayfield West, NSW 2304, Australia.

For a 27 wt pct Cr–2.53 wt pct C HCCI, Guitar et al.[26] have shown from thermodynamic and kinetic calculations that M_7C_3 secondary carbides precipitate during heating to the destabilization temperature. While holding at 980 °C, the carbides completely transform into $M_{23}C_6$. Their simulated results also showed that further precipitation of $M_{23}C_6$ occurred during cooling in the temperature range of 980 °C to 750 °C. Nevertheless, based on their experimental results, after destabilization at 980 °C during 1.5 hours followed by air cooling, only $M_{23}C_6$ is observed. There is no clear evidence that M_7C_3 forms first and then fully transforms to $M_{23}C_6$ throughout the holding, as concluded by the authors. The sequence of precipitation from M_7C_3 to $M_{23}C_6$ is also supported by Inoue and Masumoto[27] in their study on steel containing 18 wt pct Cr, 3.6 wt pct C, and 3-8 wt pct tungsten or molybdenum. They showed that tempering above 600 °C, realized after solidification, gave rise to the transformation sequence $M_3C \rightarrow M_7C_3 \rightarrow M_{23}C_6 \rightarrow M_6C$.

On the other hand, Wang et al.[24] have shown that initial secondary carbides that precipitate during destabilization of 16Cr–2.77C–1Mo–1Cu HCCI alloy correspond to $M_{23}C_6$. They identified two types of $M_{23}C_6$: one with a square-shaped morphology presenting a cube-cube orientation with the matrix and one with a grainy morphology with no specific orientation. The latter had most likely been formed during the cooling stage of the destabilization process. They also observed that longer holding times result in the transformation of the $M_{23}C_6$ secondary carbides into M_7C_3 rods. Powell and Bee[25] report a similar precipitation sequence in their work on destabilizing an 18Cr–3.1C–1.1Mo white iron. Short destabilization treatment of 15 minutes at 1000 °C results in square-shaped $M_{23}C_6$ secondary carbides formation. After holding for 4 hours at 1000 °C, a mixture of $M_{23}C_6$ and M_7C_3 secondary carbides was formed. Furthermore, and to add to the debate concerning secondary carbide formation, the authors precise that $M_{23}C_6$ secondary carbides were not predicted by equilibrium considerations. They explain it due to the good lattice matching between austenite and $M_{23}C_6$.

These studies highlight that discrepancies still exist regarding the precipitation of secondary carbides. In this work, the destabilization treatment and its influence on the microstructure and hardness of a 23 wt pct Cr–2.7 wt pct C HCCI alloy is investigated. The aim is to investigate more in detail the secondary carbides formation sequence for intermediate Cr/C ratio associated with an intermediate Cr content. The formation of secondary carbides and matrix phase transformation is characterized by dilatometry and microscopy to better understand the phase transformations occurring during destabilization treatment. Furthermore, the hardness evolution is characterized and related to the microstructure modification occurring due to the destabilization treatment.

II. MATERIAL AND EXPERIMENTAL PROCEDURES

The study has been performed on a hypoeutectic high-chromium cast iron containing 23 wt pct Cr–2.7 wt pct C (+ Mo), which is in the composition range of the ASTM A532, Class III, type A. The material was cast as a 300 kg ingot prepared by the conventional casting method, where the melt was poured into a sand mold and cooled naturally to ambient temperature. The final ingot shape consisted of a trapezoidal prism (500 mm high, 350 mm wide, and bases of 358 mm and 100 mm long). The ingot was sectioned using wire-electrode cutting. Due to the size of the ingot, there is a significant difference in solidification rate throughout the entire ingots, directly affecting the microstructure. All specimens were extracted from the same location (top of the ingot, in the edge position) to have a comparable initial microstructure for all specimens. Samples were extracted and cut into cylindrical specimens for dilatometry (Ø 4 × 10 mm). Microstructural characterization and mechanical testing were conducted on these dilatometry samples. These specimens were mounted, ground, and polished following standard metallographic procedure and final polishing with colloidal silica suspension (0.06 μm). composition

Dilatometric measurements were performed in a TA Instruments DIL 805 A/D dilatometer. Specimens were subjected to destabilization treatment at 820 °C, 910 °C, and 1000 °C for 2, 5, and 10 hours (conditions used are summarized in Table I). Samples were heated at 5 °C/minute and cooled down to room temperature (RT) using an argon-flow controlled cooling rate of 5 °C/minute. The actual temperature during the experiment was recorded using a type-S thermocouple brazed to the sample surface.

The microstructure was examined with a Jeol JSM 7800F field emission gun scanning electron microscope (FEG-SEM) equipped with an OXFORD X-Max energy dispersive (EDS) X-ray Spectrometer detector. The fraction of eutectic carbide was determined from SEM images, by image analysis using ImageJ software, from an average of 10 micrographs per sample. Electron Backscatter Diffraction (EBSD) and EDS of the specimen were examined simultaneously and analyzed using AZtec software. X-Ray diffraction (XRD) analyses were performed to determine the constituent phases using a PANalytical X'Pert MRD XL laboratory diffractometer with a Cu source, an acceleration voltage of 40 kV, and a 40 mA tube current. The diffraction data were collected over a 2θ range from 35 to 105 deg, scanned with a step width of 0.02 deg and a counting time of the 20 seconds per step. For the as-cast state, phase quantification was performed using Rietveld refinement.[28] Transmission Electronic Microscopy (TEM) analyses were performed to image the secondary carbides, using a JEOL 2100F FEG-TEM operating at an accelerating voltage of 200 kV. TEM thin foils were prepared by Focused Ion Beam on a FEI Quanta 3D FEG (FIB-SEM).

Table I. Heat-Treatment Conditions

Specimen Code	Temperature (°C)	Holding Time (h)
1A	820	2
2A		5
3A		10
1B	910	2
2B		5
3B		10
1C	1000	2
2C		5
3C		10

Characterization of mechanical properties was performed using hardness and nano-indentation measurements. The bulk-hardness of the samples was measured from Vickers micro-hardness testing with Struers Durascan equipment. Measurement was performed using a load of 98.07 N (HV10) and a dwell time of 15 seconds. The mean values for each point are based on 15 measurements. Load control mode nano-indentation was performed using a Hysitron TI950 Tribo-Indenter equipped with a Berkovich diamond indenter (tip radius of 150 nm) and at an applied load of 5 mN. The indenter area function and tip radius were determined using a calibration material (fused silica), and the area function was calculated using the Oliver and Pharr method. A 10×20 indentation grid with a step of 20 μm was performed on specific areas of microstructural interest, specifically large areas containing at least a dendrite. This allowed the characterization of the applied heat treatment's effect on the matrix's hardness and eutectic carbides.

III. RESULTS

A. As-Cast Microstructure

The as-cast microstructure (Figure 1) consists of primary austenite dendrites and M_7C_3 eutectic carbides (M = Cr, Fe). The SEM images and phase map reveal the matrix phase to be fully martensitic surrounding eutectic carbides. In contrast, the dendrites are composed of a mixture of martensite and austenite, where the martensite is located around the perimeter of the dendrite, and the core of the dendrite is mainly austenite. This type of dual-phase dendritic structure is due to the depletion of carbon and chromium during eutectic carbide formation, facilitating martensite formation.[1,25,29]

The fraction of eutectic carbide determined from image analyses is 28 ± 2 pct. This value is close to the approximate carbide volume fraction (CVF) calculated using the formula developed by Maratray and Usseglio-Nano,[30] given in Eq. [1], equal to 25.7 vol pct :

$$\text{pct CVF} = 12.33(\text{pctC}) + 0.55(\text{pctCr}) - 15.2 \quad [1]$$

where pct C and pct Cr correspond to the weight percent of C and Cr, respectively.

The observed microstructure is also consistent with the XRD analysis (see Figure 2). Quantification of the phase, obtained by Rietveld refinement, gives an approximate volume fraction of 28.9 ± 0.9 vol pct and 10.6 ± 0.6 vol pct for eutectic carbide and austenite, respectively.

B. Phase Transformation During Destabilization Treatments

During the heating of the sample in the dilatometer, the change in length (ΔL) and temperature (T) as a function of time were recorded, from which $\Delta L/L_0$ vs T was plotted (L_0 being the initial length of the sample). The dilatometry curve obtained for a thermal cycle consisting of a heating rate from ambient to 1000 °C at 5 °C/min, a 2 hours destabilization hold at 1000 °C, and finally cooled to ambient at 5 °C/minute is given in Figure 3(a). A more explicit representation of the transformations during the continuous heating can be seen from the first derivative of the relative dimensional change with respect to temperature (Figure 3(b)). Three transformations can be identified during the heating stage. The first transformation is detected at ~ 550 °C. This phenomenon is most likely to be secondary carbide precipitation, confirmed in SEM and TEM images presented below. The second transformation, observed at ~ 710 °C, is due to the magnetic transition, as indicated by an increase in the power of the inductor (Figure 3(b)).[31,32] The third transformation is characterized by a significant contraction and indicates austenite formation. The contraction is due to the higher packing density of the face-centered cubic (fcc) austenitic phase compared to the body-centered cubic (bcc) ferrite or martensite phase. The austenite transformation's starting (Ac1) and finishing temperatures (Ac3) were determined to be 772 °C and 886 °C, respectively.

The signal corresponding to continuous cooling is given in Figure 3(c). On the figure, the dilatometry curve and its first derivative are presented after holding 2 hours at 820 °C, 910 °C, or 1000 °C. In all cases, the first derivative curves show that the rate of contraction drops slightly
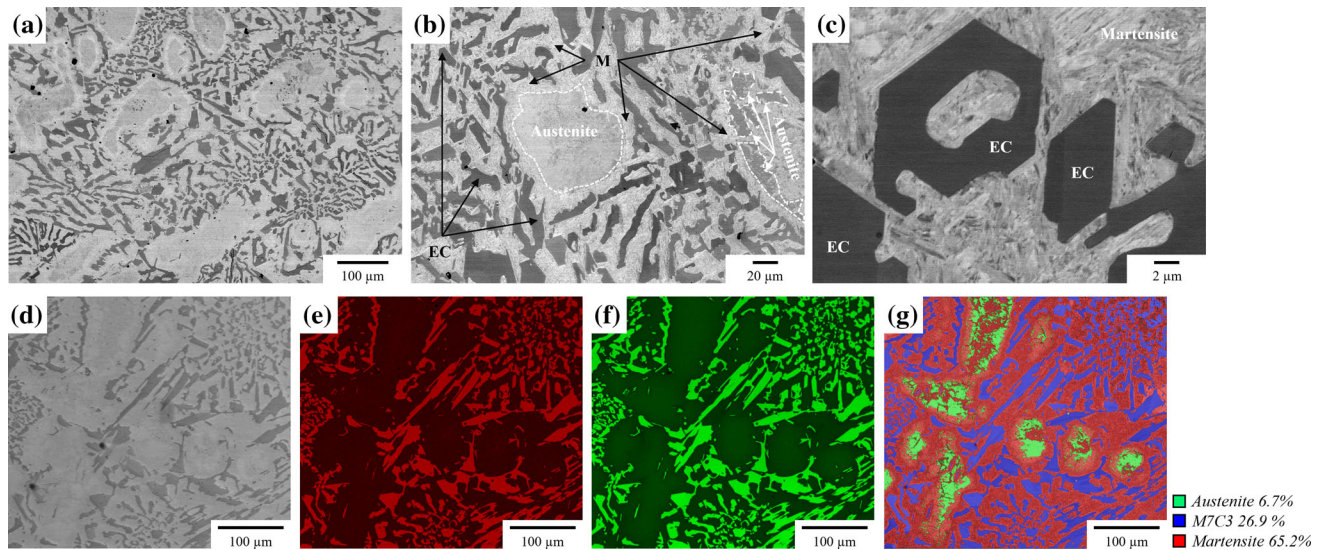
Fig. 1—SEM micrographs of the as-cast microstructure showing (*a, d*) the general view of the microstructure, (*b*) dendritic structure with a more detailed observation of eutectic carbides (EC), austenite and martensite (M), (*c*) higher magnification image of the eutectic carbides morphology, and the distribution of (*e*) C, (*f*) Cr, and (*g*) phase map obtained by EDS and EBSD.
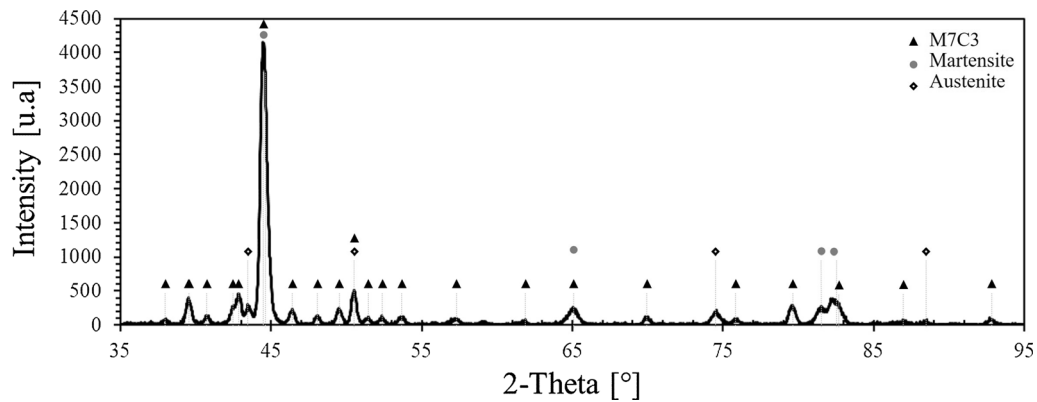

Fig. 2—X-ray pattern corresponding to the as-cast state.

before attaining a uniform value in the range of 500 °C to 600 °C. Prior to this, the non-linear contraction may indicate carbide precipitation occurring during cooling. The start of the martensite reaction is clear and is indicated by a significant expansion of the dilatometric curves. Irregular expansions and contractions are seen during the martensitic transformation (highlighted by the first derivative), particularly after the 820 °C and 910 °C destabilization treatments. This can be explained by chemical inhomogeneities in the austenitic phase, which are less marked after the higher temperature destabilization.

The evolution of martensite start (M_s) temperature according to the destabilization heat treatments is given in Figure 4. M_s was determined from the dilatometric curve based on the tangent method, according to ASTM A1033-18.[33] The results show a decrease in M_s with an increase in destabilization temperature. Overall, increasing the holding time has only a small impact on M_s. These results will be further discussed and explained in the discussion section.

C. *Microstructure Evolution After Destabilization Heat Treatments*

After all destabilization treatments, the microstructures consist of dendritic regions composed of martensite and secondary carbides and inter-dendritic regions composed of morphologically-modified eutectic carbides and martensite. The eutectic carbides show indeed a change in morphology with increasing destabilization temperature, with notably rounded corners seen at higher temperatures (see Figure 5). Furthermore, the quantification of EC, presented in Table II, reveals a slight reduction of eutectic carbides fraction with the increase of holding time at 910 °C and 1000 °C.

For destabilization at 820 °C, SEM and TEM observations reveal secondary carbides precipitated in the dendritic region within the martensite matrix, with a square-shaped (Figures 6 and 7). The selected area diffraction (SAED) patterns (see Figure 7) show that the secondary carbides display a cubic structure for this
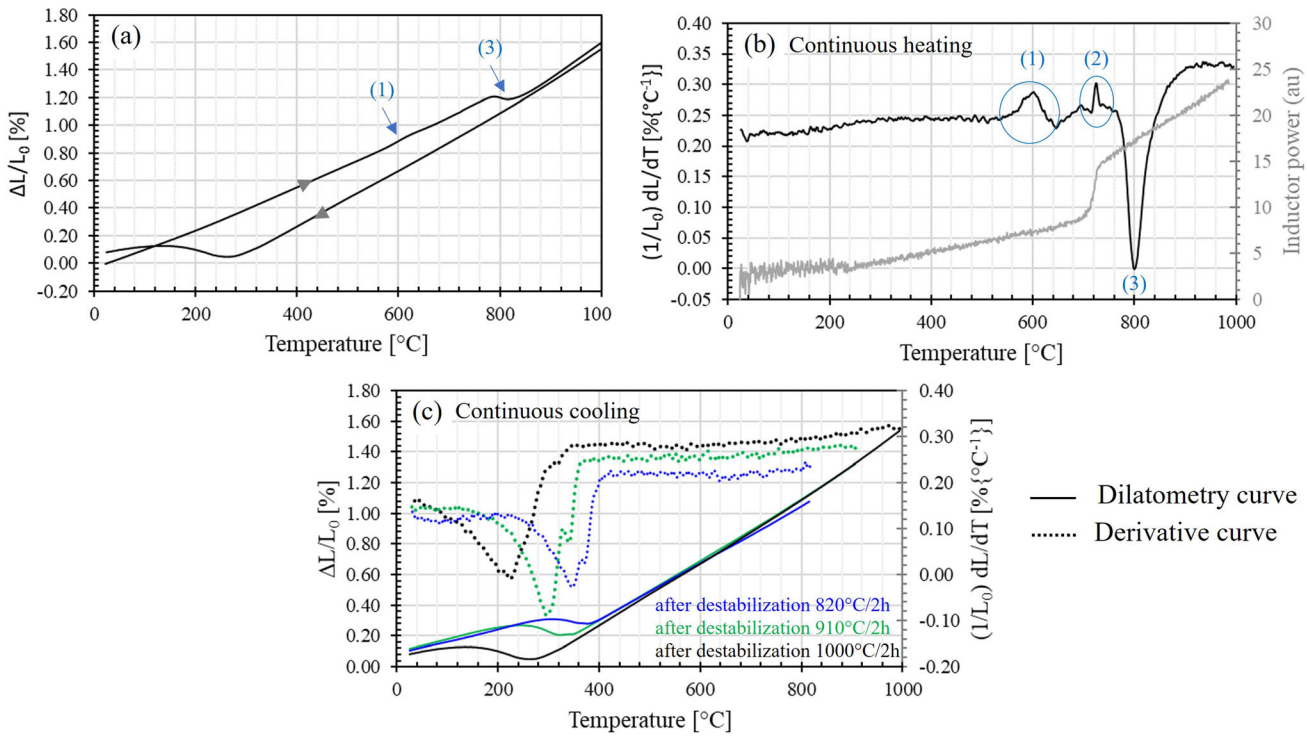
Fig. 3—(*a*) Evolution of relative change of length with temperature obtained during heating and cooling at 5 °C/min, for a thermal cycle at 1000 °C during 2 h, (*b*) corresponding derivative and inductor power evolution during continuous heating at 5 °C/min, (*c*) relative change of length and derivative signals obtained during the continuous cooling at 5 °C/min after destabilization of 2 h at 820 °C, 910 °C and 1000 °C (curve in blue, green, and black, respectively) (Color figure online).
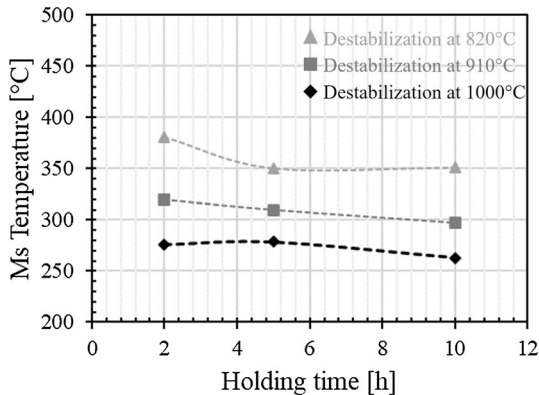

Fig. 4—M_s evolution according to holding time for destabilization treatment at 820 °C, 910 °C, and 1000 °C.

condition, which supports their identification as $M_{23}C_6$. Their size range is 100 to 500 nm.

To clarify the chemical compositions of the carbides, scanning transmission electron microscopy- Energy Dispersive Spectroscopy (STEM-EDS) was performed for material destabilized at 820 °C and 1000 °C for 2 hours. The results are given in Table III. It is seen that the chemistry of the secondary carbides is consistent with $M_{23}C_6$ and M_7C_3 formation. The 'M' component of the $M_{23}C_6$-type carbide includes Cr, Mo, and Fe at approximately 44, 1, and 33 at pct, respectively. We can also note that the composition of $M_{23}C_6$ is similar for

both heat treatments. No M_7C_3 secondary carbides could be detected for the 820 °C treatment.

At 910 °C, only $M_{23}C_6$ secondary carbides were observed for holding times of 2 and 5 hours. In contrast, for a longer holding time of 10 hours, a mixture of two types of secondary carbides was observed, one appearing with a darker contrast in backscattered SEM imaging, shown in Figure 8. From the backscattered electron composition-contrast image (BSE) (Figures 8(d), 9(b), (c)), we can differentiate both types of secondary carbides, due to their shape and their atomic number (Z). $M_{23}C_6$ has a higher metal-to-carbon ratio in comparison to M_7C_3 (3.8 to 2.3), giving a higher average Z (see Table III). The darker carbides are thus M_7C_3. (Note that the dark periphery of certain particles in Figure 8(d) is a shadowing artifact).

At all holding times at 1000 °C, two populations of secondary carbides were also observed (Figures 9 and 10). Bright-field (BF) TEM images of secondary carbides with the corresponding selected area diffraction patterns (SADP) are presented in Figure 10. For short holding times at 1000 °C, the darker M_7C_3 secondary carbides appear to be preferentially distributed around the periphery of the dendrite, separated from the eutectic carbides by a small precipitate free zone (Figure 9(a)). With increasing holding times, the darker contrast M_7C_3 secondary carbides extend from the periphery towards the core of the dendrite (Figure 9(c)). Thus, a more homogeneous distribution of M_7C_3 in the dendrite is obtained. $M_{23}C_6$ secondary carbides are observed through the entire matrix and present mainly a
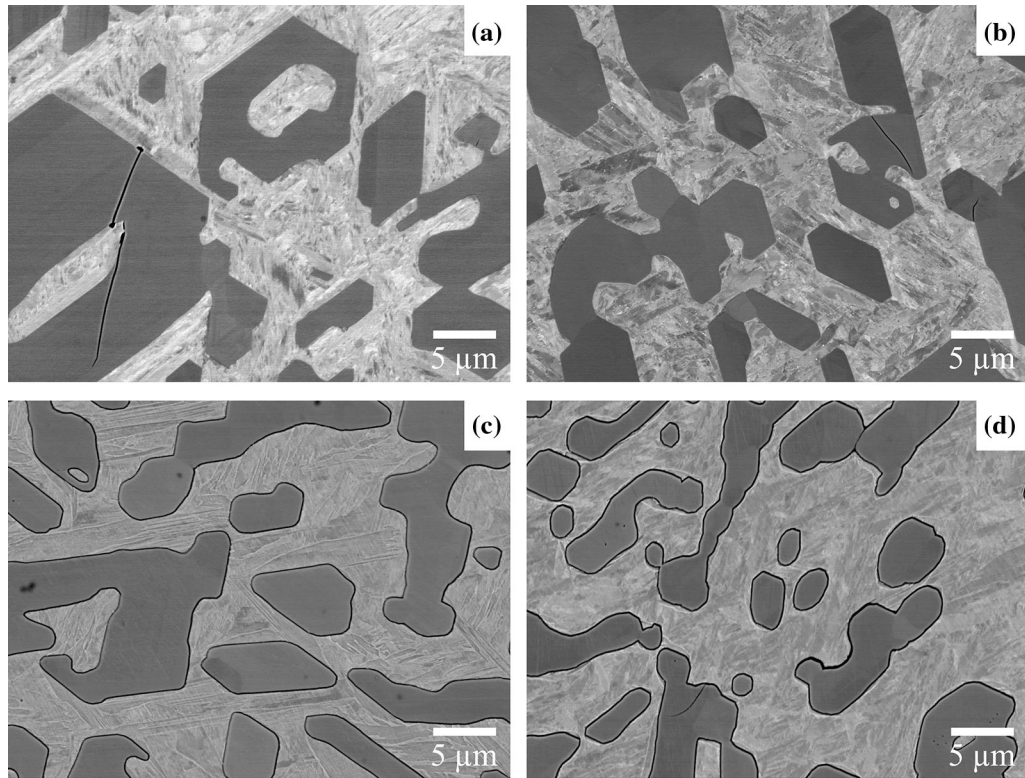
Fig. 5—Secondary electron images showing the influence of destabilization temperature on eutectic carbides morphology: (*a*) As-cast state; (*b*) 5 h at 820 °C; (*c*) 5 h at 910 °C; (*d*) 5 h at 1000 °C.

Table II. Quantification of Eutectic Carbides from Image Analyses

State	Eutectic Carbide (EC)
As-Cast	29.5 ± 2.1
(1A) 820 °C/2 h	29.2 ± 2.8
(2A) 820 °C/5 h	29.1 ± 1.7
(3A) 820 °C/10 h	29.1 ± 1.1
(1B) 910 °C/2 h	29.2 ± 1.1
(2B) 910 °C/5 h	28.9 ± 1.1
(3B) 910 °C/10 h	28.5 ± 0.9
(1C) 1000 °C/2 h	27.5 ± 1.1
(2C) 910 °C/5 h	27.2 ± 1.5
(3C) 1000 °C/10 h	26.0 ± 1.3

square-shaped (Figures 8(b), (d), 9(b), (d), 10(b)). The size of $M_{23}C_6$ secondary carbides is finer than the M_7C_3 carbides, varying from 100 to 500 nm compared to 200 to 1600 nm for M_7C_3. Furthermore, the observations show that the M_7C_3 secondary carbides tend to be elongated with an aspect ratio of ~ 0.68, and their fraction increases with the holding time at 1000 °C (see Figures 9(a) and (c)). It should be noted that no quantification of secondary carbides has been performed. Their size associated with their low phase-contrast image difference with the matrix does not allow accurate and representative measurements of the overall volume of secondary carbides. Hence, only a qualitative analysis is provided.

The austenitic phase is undetected on the XRD pattern after destabilization at 820 °C and 910 °C. Only after heat treatment at 1000 °C pics corresponding to the austenitic phase are observed. Nevertheless, their intensities are relatively low, and due to overlapping with peaks corresponding to other phases, quantification has not been done. Based on the comparison with the pattern corresponding to the AC, we can only suppose that qualitatively, the fraction of retained austenite (RA) is << 10 vol pct.

D. *Hardness and Nano-indentation*

The nanohardness distribution resulting from the indentation arrays is shown in Figure 11(a). There are two distinct peaks. The 'first' peak, corresponding to lower nanohardness values, can be ascribed to the 'matrix', and the peak seen at higher nanohardness values can be ascribed to the eutectic carbides. The breadth of the 'matrix' peak in the as-cast state reflects the contributions of austenite and martensite. Nanohardness distributions for the samples subjected to destabilization treatments at 820 °C, 910 °C, and 1000 °C for 10 hours are presented in Figures 11(b) through (d). For these heat-treated samples, the 'matrix' peak reflects the contributions of martensite and secondary carbides (as illustrated by SEM observations). The mean nanohardness values obtained are summarized in Table IV. From these measurements, we can conclude that the matrix phase nanohardness initially decreases, relative to the as-cast state, when
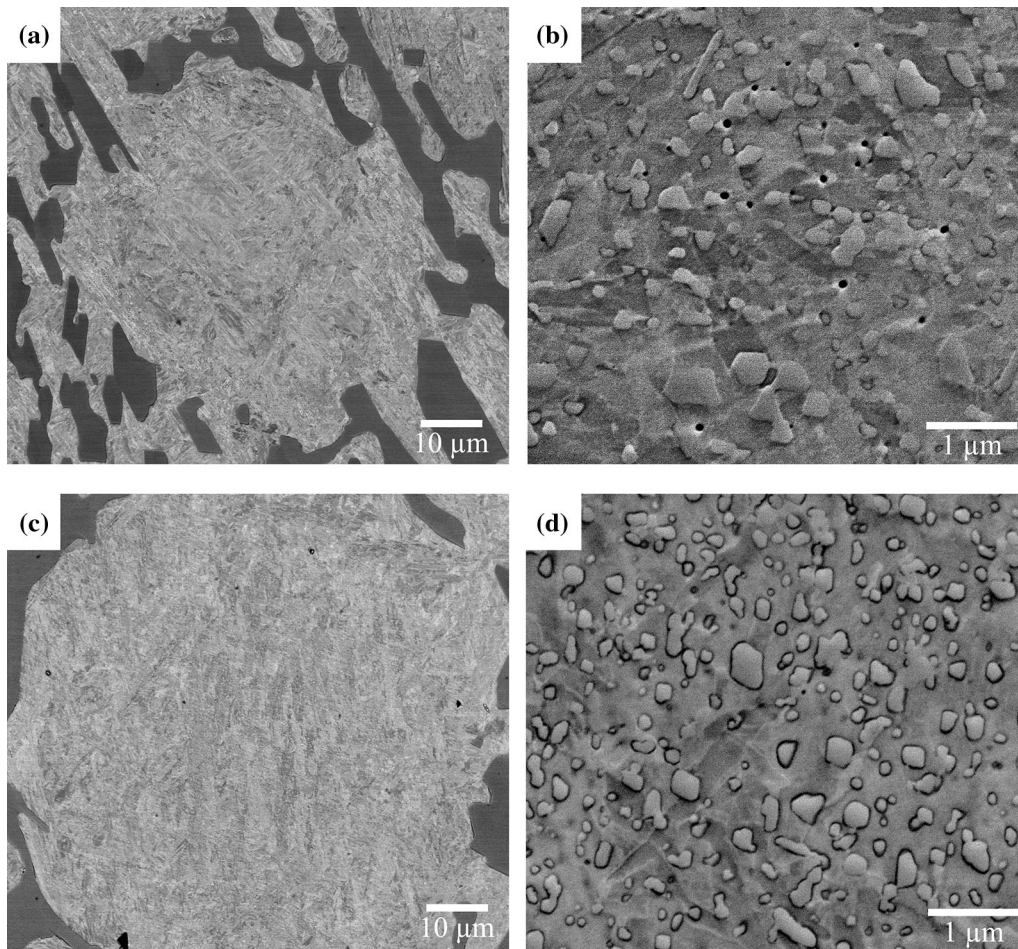
Fig. 6—Backscattered electron images showing a general view of a dendritic region and secondary carbides morphology after destabilization treatment at 820 °C for a duration of (a, b) 2 h and (c, d) 10 h.

destabilization is conducted at low temperatures (820 °C) or a moderate temperature (910 °C) for a short duration. The matrix nanohardness increased to above the as-cast matrix with a further increase in the destabilization temperature (1000 °C). The eutectic carbide nanohardness was not affected significantly by the destabilization treatment.

In the as-cast state (AC), the bulk-hardness of the alloy is ~ 600 HV10. The results obtained after destabilization treatments at 820 °C, 910 °C and 1000 °C are given Figure 12. For the lowest destabilization temperature of 820 °C, bulk-hardness decreases in comparison to the as-cast state. The comparison of heat-treated states shows an increase in hardness with destabilization temperature, and the variation with holding time is limited. The destabilization at 1000 °C results in higher bulk-hardness values. Conclusions obtained from bulk-hardness are consistent with the trend obtained from the nano-indentation tests. As mentioned, the proportion of martensite in the as-cast matrix is relatively high, and this explains why hardness modifications are subtle and not significantly affected by heat treatments, especially for treatment at the lowest temperatures of 820 °C and 910 °C. This evolution is discussed in the following section.

IV. DISCUSSION

The present study reveals the impact of destabilization treatment temperature and time on the microstructure and hardness of 23 wt pct Cr–2.7 wt pct C hypoeutectic HCCI, and allows us to sketch out the following description of the microstructure evolution.

First, the as-cast microstructure must be considered. The initial microstructure consisted of M_7C_3 eutectics carbides (around 28 vol pct) and a matrix of mixed martensite and retained austenite. The martensite is present in the vicinity of the eutectic carbides. This can be understood to be due chiefly to the carbides acting as local carbon and chromium sinks during solidification. Near the eutectic carbides, the carbon and chromium levels are sufficiently low to allow martensite to form during cooling.[8,29,34–36] Austenite is retained, mainly in the dendritic region, due to the paucity of carbides to take up carbon upon cooling. In dendritic regions, smaller eutectic carbides are also observed. There is, therefore, a considerable gradient in solute carbon content over the cast structure. The fraction of austenite retained is relatively low (around 10.6 pct) compared with most as-cast high-Cr cast irons, where the fraction is generally above 50 vol pct.[9,37,38] We explain this
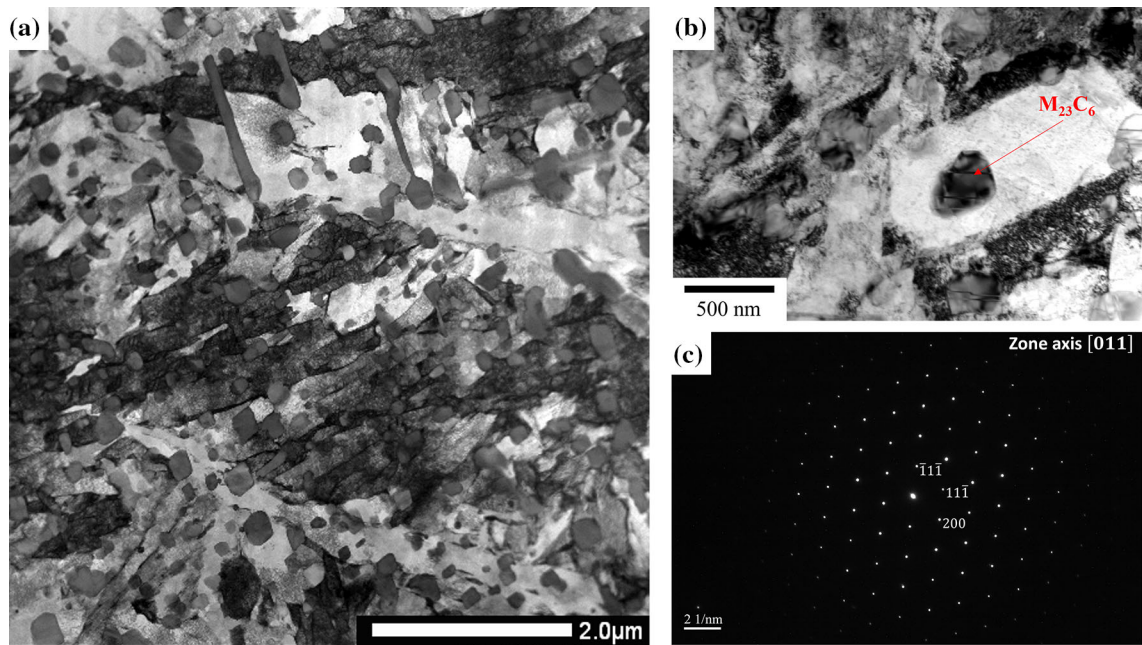
Fig. 7—(*a*) BF-TEM micrograph showing secondary carbides within the martensite matrix after destabilization at 820 °C for 2 h, (*b*) BF-TEM micrograph showing an arrow-marked secondary carbide $M_{23}C_6$, and (*c*) the corresponding SAED pattern taken from the particle in the zone axis of [011].

difference due to a slow and not controlled solidification rate.[7,39] For particularly slow solidification rates, studies report secondary carbide formation leading. In the case of the study, we could not observe secondary carbides with precision. However, we cannot exclude clustering formations, which could explain the significant proportion of martensite formed locally.

Upon heating to the destabilization temperature, which can be relatively slow in relation to the cooling rate following casting, some formation of secondary carbides occurs in carbon-rich areas. This explains the expansion/contraction peak in the dilatometry curves at 550 °C. Overall, the dominance of martensite in the observed structures following destabilization points to the success of the core aim of the treatment for all conditions. That is, to induce secondary carbide formation so as to reduce the carbon content in the carbon-rich zones of the matrix, thereby destabilizing the austenite in those regions. There is also an indication in the dilatometry curves of some secondary carbide formation during cooling.

For destabilization at 820 °C and shorter holding times at 910 °C, only $M_{23}C_6$ secondary carbides were observed. This is broadly consistent with the study of Wang *et al.*,[40] which reported that a 16Cr–2.77C–1Mo–1Cu HCCI alloy heat-treated at 580 °C for 6 to 10 hours displays only $M_{23}C_6$ secondary carbides. In the present work, M_7C_3 secondary carbides were only seen at higher destabilization temperatures. This suggests that M_7C_3 secondary carbides form in the carbon-rich zones during the hold, but only if the temperature is sufficiently high and the holding time is long enough. The $M_{23}C_6$ secondary carbides, seen in all

conditions, are typically smaller in size range than the M_7C_3 secondary carbides. The observed $M_{23}C_6$ secondary carbide size range of 100 to 500 nm is in good agreement with the values reported by Powell and Bee[25] and Wiengmoon *et al.*[15] These $M_{23}C_6$ secondary carbides most likely formed during the heating and cooling stage (see References 4, 12, and 26). For the present material, we can, therefore, reject the proposed precipitation sequence: $M_7C_3 \rightarrow M_{23}C_6$,[26,27] during holding at the destabilization temperature. Instead, we propose that the kinetics of $M_{23}C_6$ secondary carbide formation is faster relative to M_7C_3 at temperatures lower than ~ 850 °C, but that M_7C_3 formation is favored above this temperature. CALPHAD equilibrium calculations made using Thermo-Calc (Figure 13) suggest that kinetic considerations dominate at the lower temperatures, as both $M_{23}C_6$ and M_7C_3 are predicted to be stable below 850 °C. At higher temperatures, equilibrium considerations favor the formation of secondary M_7C_3 in the carbon-rich zones. Furthermore, $M_{23}C_6$ has a cubic structure. Its formation is thus thermodynamically favorable as presenting a low misfit with the matrix.[25] M_7C_3 secondary carbides are primarily observed at the periphery of the dendrite at the first stage, and by increasing the time hold at 1000 °C, they are also observed in the core of the dendrite. This sequence is similar to the finding reported in references[9,41] for a 26Cr–2.5C and 14.6Cr–2.7C white cast irons, respectively. It is also consistent with the partial dissolution of eutectic carbides observed, which results in the establishment of carbon and chromium gradient during holding across the dendrite, from the periphery toward the core of the dendrites.

Table III.   Chemical Composition of the Secondary Carbides Obtained by STEM Energy Dispersive Spectroscopy

Heat-Treatment	Phase	Chemical Composition (At Pct)						Z Average
		C	Si	Cr	Mn	Fe	Mo	
(1A) 820 °C/2 h	$M_{23}C_6$	21.24	0.34	43.78	0.37	33.23	1.04	20.70
(1C) 1000 °C/2 h	$M_{23}C_6$	21.23	0.06	43.72	0.60	33.01	1.37	20.75
	M_7C_3	30.09	0.80	23.17	0.79	44.90	0.25	17.01
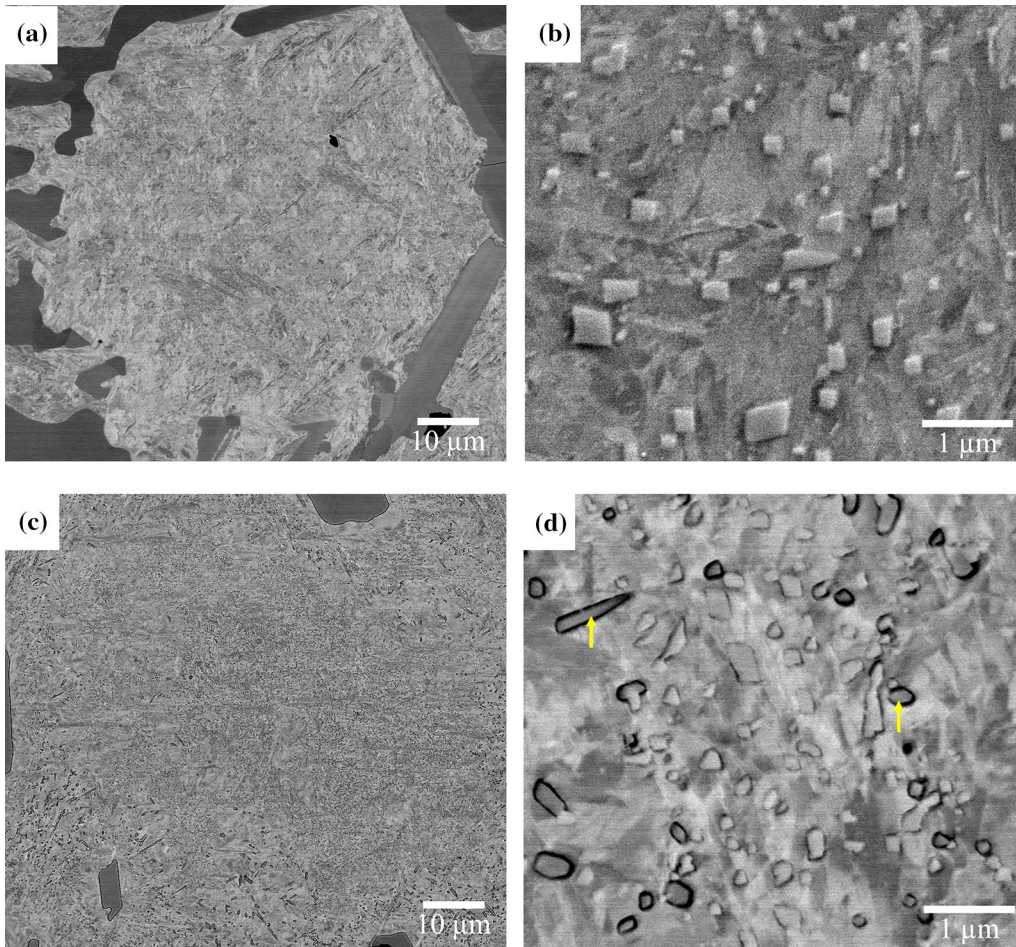
Fig. 8—Backscattered electron image showing a general view of a dendritic region and secondary carbide morphology after destabilization treatment at 910 °C at a duration of (*a*, *b*) 2 h and (*c*, *d*) 10 h. Yellow arrows indicate M_7C_3 secondary carbides (Color figure online).

The eutectic carbide morphology did not alter significantly during the present treatments, except for corner rounding at higher temperatures by partial dissolution, which is supported by the reduction of eutectic carbide fraction. This is consistent with the finding of Gonzalez-Pocino et al.,[12] who on a 3C–18Cr (wt pct) HCCI, have shown that higher holding at the destabilization of 1000 °C leads to a higher percentage of dissolved EC. They also reported that increased holding time leads to greater precipitated secondary carbides, which agrees with our results. The authors explain that the hardness increases with holding time due to a higher fraction of secondary carbides precipitated and a lower fraction of

RA. Nevertheless, they don't consider the effect of carbide dissolution on the matrix composition and, ultimately, martensite hardness. Karantzalis et al.,[1] in their study on 2.35C–18.2Cr HCCI, have observed that, for high destabilization temperature (at 1100 °C), both eutectic and secondary carbides start to dissolve in the matrix. This enhances the stability of the austenite and tends to decrease the bulk-hardness. Similarly to,[12] the authors explain the hardness evolution depending on the precipitated secondary carbides and the RA content. Hong et al.[13,42] also reported the dissolution phenomenon in their study on 2C–27.5 Cr (wt pct) HCCI. The authors have shown that eutectic carbides are first
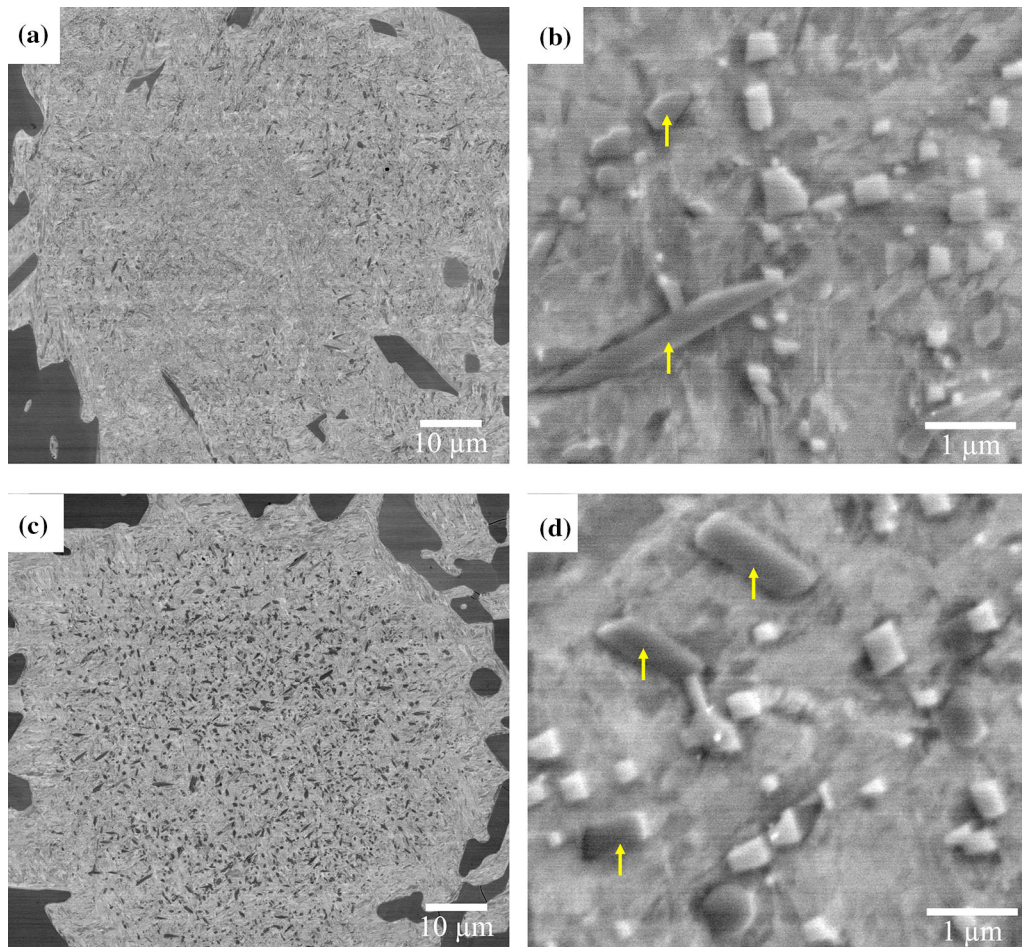
Fig. 9—Backscattered electron image showing a general view of a dendritic region and secondary carbides morphology after destabilization treatment at 1000 °C at a duration of (*a, b*) 2 h and (*c, d*) 10 h. Yellow arrows indicate M_7C_3 secondary carbides (Color figure online).
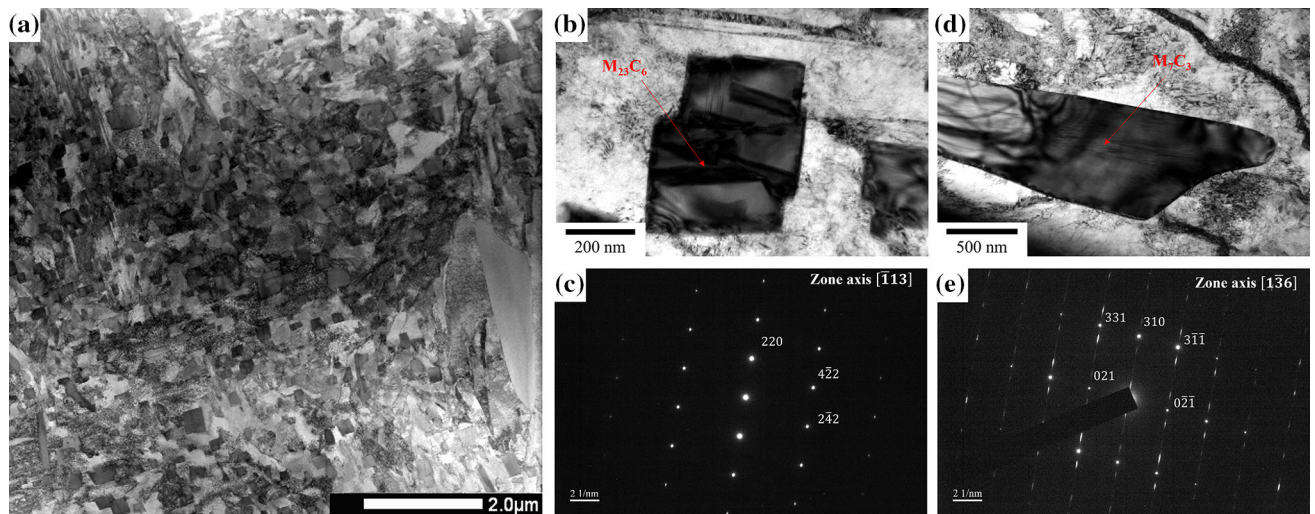

Fig. 10—(*a*) BF-TEM micrograph showing secondary carbides within the martensite matrix after destabilization at 1000 °C for 2 h, (*b*) BF-TEM micrograph showing an arrow-marked secondary carbides $M_{23}C_6$, and (*c*) the corresponding SAED pattern taken from the particle in the zone axis of [-113]. (*d*) BF-TEM micrograph showing arrow-marked secondary carbides M_7C_3 and (*e*) the corresponding SAED pattern taken from the particle in the zone axis of [1-36].
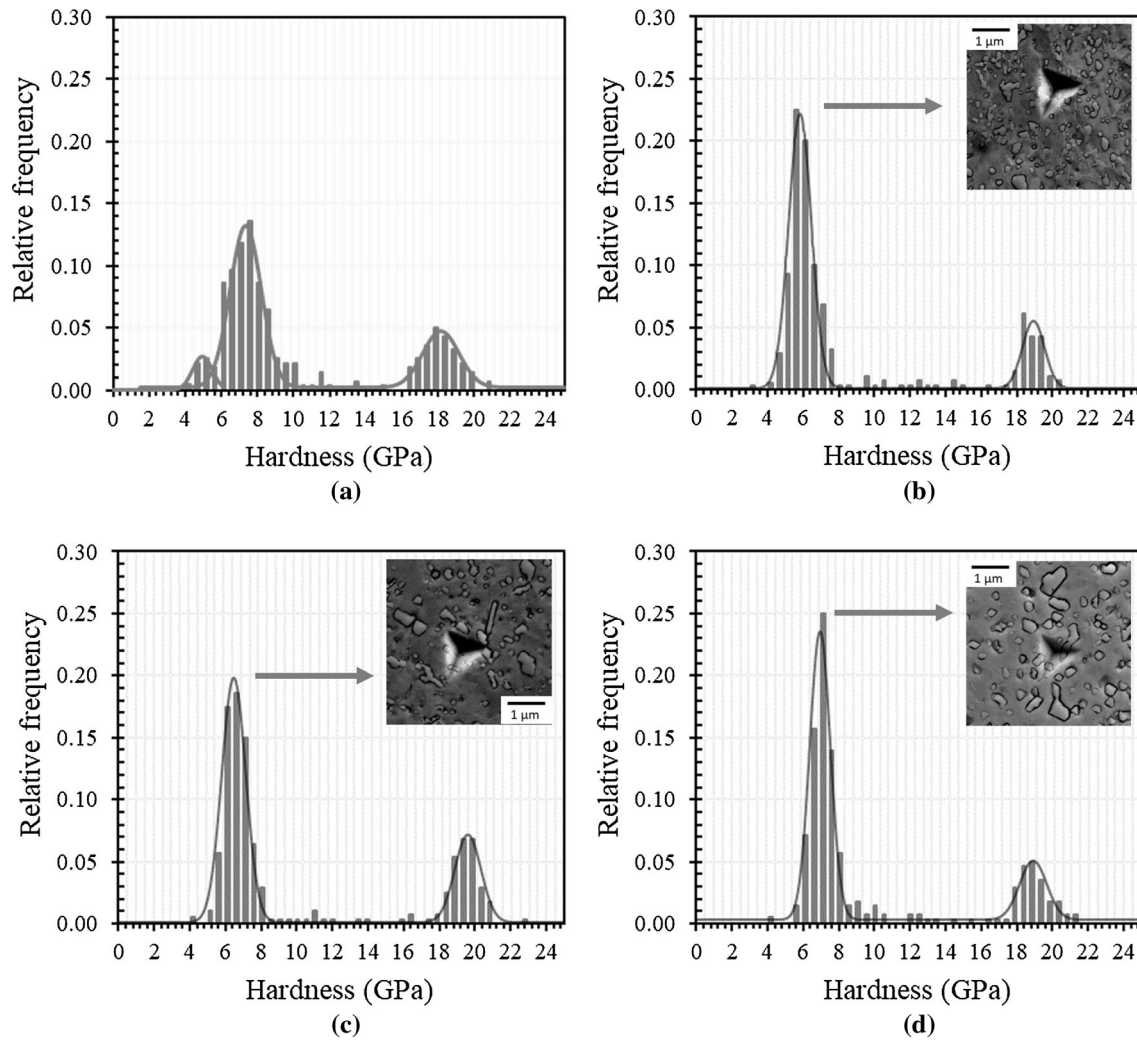
Fig. 11—Nanohardness distribution measured on (*a*) the as-cast state and after destabilization treatment of 10 h (*b*) at 820 °C, (*c*) at 910 °C and (*d*) at 1000 °C.

Table IV. Nanohardness Values from Nano-indentation Tests for the Constituent Phases After Various Destabilization Treatments (GPa)

State	'Matrix'	Eutectic Carbide (EC)
As-Cast	6.3 ± 0.6	18.2 ± 0.9
(1A) 820 °C/2 h	5.7 ± 0.8	19.2 ± 0.5
(3A) 820 °C/10 h	5.8 ± 0.8	18.9 ± 0.5
(1B) 910 °C/2 h	5.9 ± 0.9	18.0 ± 0.9
(3B) 910 °C/10 h	6.5 ± 0.8	19.6 ± 0.9
(1C) 1000 °C/2 h	7.0 ± 0.6	18.7 ± 0.9
(3C) 1000 °C/10 h	7.0 ± 0.7	18.9 ± 0.9

expanded (destabilization around 880 °C to 1000 °C), then dissolved into the matrix (1050 °C to 1100 °C). This phenomenon leads to a Cr, C-rich matrix and serves to form secondary carbides (reported to precipitate at 900 °C). At 1100 °C, secondary carbides also start to dissolve in the matrix, stabilizing the austenite (RA ~ 21 pct). The authors explain matrix hardness evolution after destabilization treatment due to the
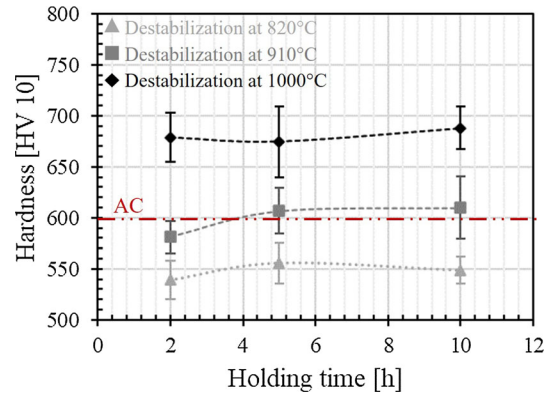

Fig. 12—Hardness values as a function of the holding time at destabilization temperatures of 820 °C, 910 °C, and 1000 °C—AC refers to the as-cast state.

precipitation and growth of secondary carbides and the matrix's enrichment with carbon and chromium.
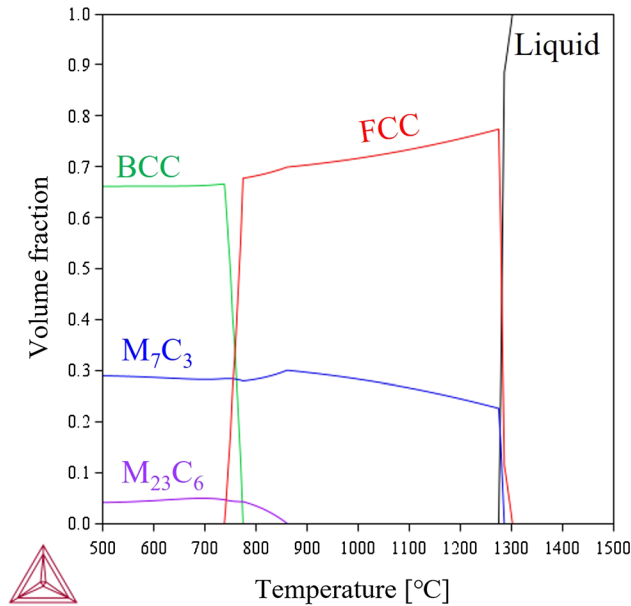
Fig. 13—Equilibrium phase fraction for the studied HCCI alloy calculated using Thermo-Calc software (TCFE9, version 2022a).

When both eutectic and secondary carbides start to dissolve in the matrix, it is well understood that a decrease in the matrix's hardness (and subsequent bulk-hardness) is due to an increase in RA (stabilized by C, Cr). However, the partial dissolution of eutectic carbides and its effect on the matrix's hardness aren't clearly reported and explained. Especially when the matrix's composition does not change enough to stabilize austenite (RA fraction is relatively low (<< 10 vol pct)).

Local dissolution serves to increase the carbon content of the matrix of the dendritic region in the vicinity of the eutectic carbide region. The level of carbon in the matrix is the determining factor in the final hardness and the martensite start temperature (M_s). Due to the complexity of the microstructure, notably with the fine dispersion of secondary carbides through the martensite matrix, it is challenging to quantify the carbon of the matrix with accuracy using techniques such as EDS or EPMA. Hence, an estimation of the matrix composition, including carbon, was obtained from CALPHAD equilibrium calculations (Thermo-Calc software, TCFE9 database). We assume the possible supplementary formation of secondary carbides during cooling is of low fraction and can be neglected. To support the position that destabilization temperature establishes the martensite carbon content, and thus determines the M_s and matrix hardness values, we have used the austenite composition derived from Thermo-Calc. Calculations are done at the studied destabilization temperatures (TC@destab T°C).

M_s temperatures are calculated using the relationship developed and reported in the work of Barbier,[43] with x pct corresponding to the composition of alloying elements in the austenitic phase in mass percent (obtained from Thermo-Calc):

$$
\begin{aligned}
M_s = {} & 545 - 601.2 \times (1 - \mathrm{Exp}(-0.868\,\mathrm{C\,pct})) \\
& - 34.4\,\mathrm{Mn\,pct} - 17.7\,\mathrm{Si\,pct} - 9.2\,\mathrm{pct\,Cr} \\
& - 17.3\,\mathrm{pct\,Ni} - 15.4\,\mathrm{Mo\,pct} + 10.8\,\mathrm{V\,pct} \\
& + 4.7\,\mathrm{Co\,pct} - 1.4\,\mathrm{Al\,pct} - 16.3\,\mathrm{Cu\,pct} \\
& - 361\,\mathrm{Nb\,pct} - 2.44\,\mathrm{Ti\,pct} - 344\,\mathrm{B\,pct} \qquad [2]
\end{aligned}
$$

Table V reveals good agreement between experimental and calculated values of M_s. We can thus conclude that destabilization leads to near equilibrium levels within the austenite. It also confirms the applicability of using Thermo-Calc to estimate the carbon content in the matrix. We can then propose that the amount of eutectic carbide dissolution is an important parameter in determining the subsequent structure development. This is most likely the source of carbon increase in the matrix. Therefore, the evolution of M_s obtained experimentally with the increase of destabilization temperature is consistent with carbon evolution in the matrix. This factor is also critical to understanding the influence of destabilization temperature on the hardness.

The influence of carbon content on martensite hardness is well-known. To assess the role of this relationship in determining the present hardness levels, a few additional destabilization treatments were conducted at 950 °C, 980 °C, and 1050 °C for 5 hours. For each condition, the level of carbon in the austenite was estimated using Thermo-Calc. The measured hardness values are plotted against the estimated carbon content of the matrix in Figure 14. There is clearly a strong relationship between the matrix hardness and the predicted carbon content of the matrix. The evolution of the bulk-hardness with the carbon content presents a similar trend. As both curves are quasi-parallel and the volume fraction of eutectic carbides is not significantly modified with heat treatment (26 to 29.5 pct), we can conclude that ΔHV (bulk – matrix) is related to the contribution of EC. These results confirm that the carbon level of the austenite at the destabilization temperature is the main factor affecting hardness evolution in the present material, and the direct contribution to the hardness of the secondary carbides may be considered negligible.

At low destabilization temperatures, the matrix is impoverished in carbon due to limited eutectic carbide dissolution and intensive precipitation of $M_{23}C_6$, which explain the highest M_s temperature, and the lowest hardness level obtained. This behavior was discussed by Tabrett et al.[7] in their extensive review of high-Cr cast irons. By increasing the destabilization temperature, partial dissolution of eutectic carbides occurs causing carbon enrichment of the austenite phase and a harder martensite phase upon cooling[9] transformed at a lower temperature.

V. CONCLUSION

In response to discrepancies in the literature regarding carbide formation sequence and evolution, the present study sought to clarify the influence of destabilization

Table V. M_s Experimental, Calculated and C in Austenitic Phase Obtained from Thermo-Calc (TCFE9, Version 2022a)

Destabilization Treatment	M_s from Dilatometry (°C)	M_s Calculated (°C)	C in Austenitic Phase from TC@detab. T°C (Wt Pct)
(3A) 820 °C/10 h	351	355	0.15
(3B) 910 °C/10 h	297	302	0.24
(3C) 1000 °C/10 h	263	237	0.36
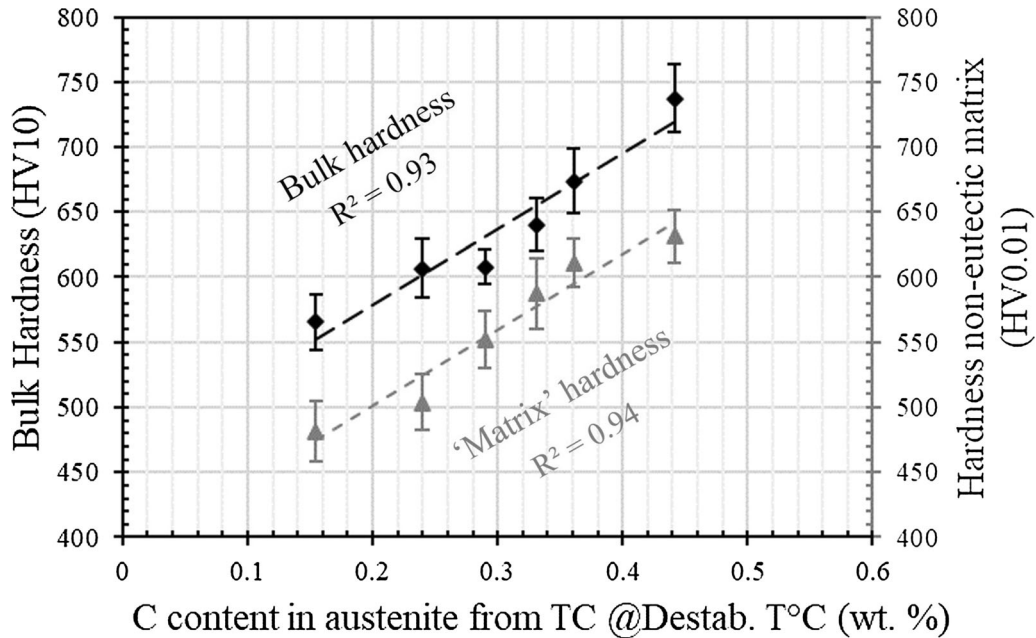
Fig. 14—Evolution of bulk-hardness and matrix hardness in relation to C content in the matrix (estimation form TC).

treatment on the microstructure and hardness of a hypoeutectic high-chromium cast iron containing 2.2 wt pct C and 16.5 wt pct Cr.

1. Starting from an inhomogeneous as-cast microstructure consisting of ~ 28 pct M_7C_3 eutectic carbide and a mixed matrix of martensite and retained austenite, destabilization treatments resulted in the establishment of near homogeneous structure with a near equilibrium level of carbon in the matrix which fully transformed to martensite upon cooling.
2. Homogeneously distributed $M_{23}C_6$ secondary carbides with a square shape 100 to 500 nm in size precipitated during heating up to the destabilization temperature.
3. M_7C_3 secondary carbides formed along with $M_{23}C_6$ with a distinctly different morphology for higher destabilization temperatures.
4. The carbon content of the matrix controls the martensite start temperature and has a dominating influence on matrix and bulk hardness.

CONFLICT OF INTEREST

On behalf of all authors, the corresponding author states that there is no conflict of interest.

FUNDING

OPEN ACCESS

REFERENCES

1. A.E. Karantzalis, A. Lekatou, and E. Diavati: *J. Mater. Eng. Perform.*, 2009, vol. 18, pp. 1078–85.
2. A. Bedolla-Jacuinde, L. Arias, and B. Hernández: *J. Mater. Eng. Perform.*, 2003, vol. 12, pp. 371–82.
3. H. Gasan and F. Erturk: *Metall. Mater. Trans. A*, 2013, vol. 44A, pp. 4993–5005.
4. J. Wang, J. Xiong, H. Fan, H.S. Yang, H.H. Liu, and B.L. Shen: *J. Mater. Process. Technol.*, 2009, vol. 209, pp. 3236–40.
5. K.A. Kibble and J.T.H. Pearce: *Cast Met.*, 1993, vol. 6, pp. 9–15.
6. C.P. Tabrett and I.R. Sare: *Scripta Mater.*, 1998, vol. 38, pp. 1747–53.
7. C.P. Tabrett, I.R. Sare, and M.R. Ghomashchi: *Int. Mater. Rev.*, 1996, vol. 41, pp. 59–82.
8. J.T.H. Pearce: *J. Mater. Sci. Lett.*, 1983, vol. 2, pp. 428–32.
9. U.P. Nayak, F. Schäfer, F. Mücklich, and M.A. Guitar: *Met. Mater. Int.*, 2023, vol. 29, pp. 934–47.
10. A. Wiengmoon, J.T.H. Pearce, S. Nusen, and T. Chairuangsri: *Micron*, 2021, vol. 143, p. 103025.
11. A. Wiengmoon, J.T.H. Pearce, and T. Chairuangsri: *Mater. Chem. Phys.*, 2011, vol. 125, pp. 739–48.
12. A. Gonzalez-Pocino, F. Alvarez-Antolin, and J. Asciensio-Lozano: *Metals (Basel)*, 2019, vol. 9, p. 522.
13. H.D.T. Hong, H.N. Hong, M.N. Ngoc, and Q.H.T. Ngoc: *ISIJ Int.*, 2021, vol. 61, pp. 1660–68.
14. Y.-G. Song, J.-S. Oh, B.-G. Choi, C.-Y. Jo, and J.-H. Lee: *Metals (Basel)*, 2021, vol. 11, p. 1690.
15. A. Wiengmoon, T. Chairuangsri, and J.T.H. Pearce: *ISIJ Int.*, 2004, vol. 44, pp. 396–403.
16. A. Wiengmoon, T. Chairuangsri, A. Brown, R. Brydson, D.V. Edmonds, and J.T.H. Pearce: *Acta Mater.*, 2005, vol. 53, pp. 4143–54.
17. J.T.H. Pearce and D.W.L. Elwell: *J. Mater. Sci. Lett.*, 1986, vol. 5, pp. 1063–64.
18. A. Wiengmoon, J. Khantee, J.T.H. Pearce, T. Chairuangsri, and I.O.P. Conf: *Ser. Mater. Sci. Eng.*, 2019, vol. 474, p. 012041.
19. M.A. Guitar, S. Suárez, O. Prat, M. Duarte Guigou, V. Gari, G. Pereira, and F. Mücklich: *J. Mater. Eng. Perform.*, 2018, vol. 27, pp. 3877–85.
20. G.L.F. Powell and G. Laird: *J. Mater. Sci.*, 1992, vol. 27, pp. 29–35.
21. S. Zhou, Y. Shen, H. Zhang, and D. Chen: *Chin. J. Mech. Eng. (English Ed)*, 2015, vol. 28, pp. 140–47.
22. S.D. Carpenter, D. Carpenter, and J.T.H. Pearce: *Mater. Chem. Phys.*, 2007, vol. 101, pp. 49–55.
23. M.J. Huq, K. Shimizu, K. Kusumoto, R.H. Purba, Y. Gaqi, *Int. J. Met.* (2023).
24. J. Wang, C. Li, H. Liu, H. Yang, B. Shen, S. Gao, and S. Huang: *Mater Charact*, 2006, vol. 56, pp. 73–78.
25. G.L.F. Powell and J.V. Bee: *J. Mater. Sci.*, 1996, vol. 31, pp. 707–11.
26. M.A. Guitar, U.P. Nayak, D. Britz, and F. Mücklich: *Int. J. Met.*, 2020, vol. 14, pp. 755–65.
27. A. Inoue and T. Masumoto: *Metall. Trans. A*, 1980, vol. 11, pp. 739–47.
28. Q. Hou, Z. Huang, and J. Wang: *J. Iron. Steel Res. Int.*, 2009, vol. 16, pp. 33–38.
29. S.D. Carpenter, D. Carpenter, and J.T.H. Pearce: *Mater. Chem. Phys.*, 2004, vol. 85, pp. 32–40.
30. F. Maratray, R. Usseglio-Nanot, Climax SA Paris Publ. (1970).
31. M. Hunkel, H. Surm, and M. Steinbacher: *Handb. Therm. Anal. Calorim.*, 2018, vol. 6, pp. 103–29.
32. A. Verma, M. Sundararaman, J.B. Singh, S.A. Nalawade, Meas. Sci. Technol. 21 (2010).
33. A.– 18, ASTM Comm. Steel, Stainl. Steel Relat. Alloy (2004) 1–14.
34. G. Laird and G.L.F. Powell: *Metall. Trans. A*, 1993, vol. 24, pp. 981–88.
35. A. Bedolla-Jacuinde, R. Correa, J.G. Quezada, and C. Maldonado: *Mater. Sci. Eng. A*, 2005, vol. 398, pp. 297–308.
36. A.E. Karantzalis, A. Lekatou, and H. Mavros: *J. Mater. Eng. Perform.*, 2009, vol. 18, pp. 174–81.
37. A. Bedolla-Jacuinde, F.V. Guerra, A.J. Guerrero-Pastran, M.A. Sierra-Cetina, and S. Valdez-Medina: *Wear*, 2021, vol. 476, p. 203675.
38. J. Wang, Z. Sun, R. Zuo, C. Li, B. Shen, S. Gao, and S. Huang: *J. Mater. Eng. Perform.*, 2006, vol. 15, pp. 316–19.
39. N.H. Kinh Luan, K. Koizumi, K. Mizuno, Y. Yamada, and T. Okuyama: *Mater. Trans.*, 2019, vol. 60, pp. 2475–80.
40. J. Wang, R.L. Zuo, Z.P. Sun, C. Li, H.H. Liu, H.S. Yang, B.L. Shen, and S.J. Huang: *Mater Charact*, 2005, vol. 55, pp. 234–40.
41. V.G. Efremenko, Y.G. Chabak, and M.N. Brykov: *J. Mater. Eng. Perform.*, 2013, vol. 22, pp. 1378–85.
42. Q.H. Thi Ngoc, N.T. Vu Diem, V.N. Hoang, H.N. Hong, H. Le Thu, and N.N. Duong: *Mater. Trans.*, 2022, vol. 63, pp. 170–75.
43. D. Barbier: *Adv. Eng. Mater.*, 2014, vol. 16, pp. 122–27.